Journal of Colloid and Interface Science 376 (2012) 296–306

Contents lists available at SciVerse ScienceDirect

Journal of Colloid and Interface Science

www.elsevier.com/locate/jcis

Interfacial layers from the protein HFBII hydrophobin: Dynamic surface tension, dilatational elasticity and relaxation times

Nikola A. Alexandrov [a], Krastanka G. Marinova [a], Theodor D. Gurkov [a], Krassimir D. Danov [a], Peter A. Kralchevsky [a,*], Simeon D. Stoyanov [b,c], Theodorus B.J. Blijdenstein [b], Luben N. Arnaudov [b], Eddie G. Pelan [b], Alex Lips [d]

[a] Department of Chemical Engineering, Faculty of Chemistry, Sofia University, Sofia 1164, Bulgaria
[b] Unilever Research & Development Vlaardingen, 3133AT Vlaardingen, The Netherlands
[c] Laboratory of Physical Chemistry and Colloid Science, Wageningen University, 6703 HB Wageningen, The Netherlands
[d] Unilever Research & Development, Port Sunlight, Wirral, Merseyside CH63 3JW, UK

ARTICLE INFO

Article history:
Received 17 December 2011
Accepted 12 March 2012
Available online 20 March 2012

Keywords:
HFBII hydrophobin
Surface relaxation times
Hydrophobic force
Dilatational surface elasticity
Storage and loss moduli

ABSTRACT

The pendant-drop method (with drop-shape analysis) and Langmuir trough are applied to investigate the characteristic relaxation times and elasticity of interfacial layers from the protein HFBII hydrophobin. Such layers undergo a transition from fluid to elastic solid films. The transition is detected as an increase in the error of the fit of the pendant-drop profile by means of the Laplace equation of capillarity. The relaxation of surface tension after interfacial expansion follows an exponential-decay law, which indicates adsorption kinetics under barrier control. The experimental data for the relaxation time suggest that the adsorption rate is determined by the balance of two opposing factors: (i) the barrier to detachment of protein molecules from bulk aggregates and (ii) the attraction of the detached molecules by the adsorption layer due to the hydrophobic surface force. The hydrophobic attraction can explain why a greater surface coverage leads to a faster adsorption. The relaxation of surface tension after interfacial compression follows a different, square-root law. Such behavior can be attributed to surface diffusion of adsorbed protein molecules that are condensing at the periphery of interfacial protein aggregates. The surface dilatational elasticity, E, is determined in experiments on quick expansion or compression of the interfacial protein layers. At lower surface pressures (<11 mN/m) the experiments on expansion, compression and oscillations give close values of E that are increasing with the rise of surface pressure. At higher surface pressures, E exhibits the opposite tendency and the data are scattered. The latter behavior can be explained with a two-dimensional condensation of adsorbed protein molecules at the higher surface pressures. The results could be important for the understanding and control of dynamic processes in foams and emulsions stabilized by hydrophobins, as well as for the modification of solid surfaces by adsorption of such proteins.

1. Introduction

The hydrophobins represent a class of amphiphilic proteins produced by filamentous fungi [1–3]. These proteins exhibit at least three remarkable properties. First, upon adsorption at an air/water or oil/water interface, the hydrophobins form films of high mechanical strength, as evidenced by the measured surface dilatational and shear moduli, which are markedly greater than those of other proteins. For example, the shear storage modulus, G', for hydrophobin adsorption layers at the air/water interface is about 10 and 100 times greater than the G' values measured, respectively, for β-lactoglobulin and β-casein layers; see Fig. 11 in [4].

Second, the hydrophobin adsorption layers undergo a transition from two-dimensional (2D) fluid to 2D solid (elastic membrane). For example, bubbles formed by shaking of hydrophobin solutions preserve the irregular shape they had at the moment of surface solidification [5]. For the common milk and egg proteins, the solidification of their adsorption layers usually takes several hours [6], whereas for hydrophobins this process happens much faster, e.g. 1 min at 0.005 wt.% protein concentration (see below). A detailed study on the solidification of hydrophobin adsorption layer can be found in [7], where it is established that the shear stress relaxation at fixed strain follows the Andrade's cubic-root law.

Third, the hydrophobins are "sticky" molecules. In nature, their self-assembled films coat fungal structures and mediate their attachment to surfaces. In water, the class II hydrophobins, like the HFBII that is used in the present study, form aggregates, which

* Corresponding author. Fax: +359 2 9625643.
E-mail address: pk@lcpe.uni-sofia.bg (P.A. Kralchevsky).

0021-9797/$ - see front matter © 2012 Elsevier Inc. All rights reserved.
http://dx.doi.org/10.1016/j.jcis.2012.03.031

are predominantly tetramers at mg/mL concentrations [8–11]. The formation of tetramers is driven by the attraction between the hydrophobic parts of the protein molecules. However, it is remarkable that the hydrophilic parts of the hydrophobin molecules also attract each other, which is evidenced by the strong adhesion between the surfaces of foam films [12] and emulsion drops [13] stabilized by such proteins, as well as by the attachment of hydrophobin aggregates to the adsorption layer at the solution's surface [1,5,8,12].

These unique properties of hydrophobins have found applications for stabilizing foams and emulsions [4,13–16], for immobilization of functional molecules at surfaces [17–21], and as coating agents for surface modification [19,20,22,23]. The structure of HFBII, determined from crystallized samples, shows that it is a single domain protein with dimensions $24 \times 27 \times 30$ Å [24]. It is a relatively small, cysteine rich protein with 70–100 amino acid residues. The cysteine residues form four disulfide bridges that interconnect the polypeptide chain into a rigid, compact, parallelepiped-like molecule, which is not believed to unfold upon adsorption [3,24]. Therefore, the adsorption kinetics of hydrophobins is expected to be influenced by their diffusion and interactions, rather than by conformational changes at the interface.

The adsorption dynamics and dilatational rheology of interfacial layers from proteins is investigated in relation to their application as stabilizers of emulsions and foams [25–35]. In particular, the high surface dilatational elasticity of the hydrophobin adsorption layers is expected to oppose the shrinking of the bubbles and to suppress the foam disproportionation (Ostwald ripening) [4]. The dilatational elasticity, E, of HFBII layers was determined in Langmuir-trough experiments by differentiation of surface-pressure-vs.-area isotherms, and by oscillatory measurements of the storage modulus [4].

In the present study, we apply the pendant-drop method with drop-shape analysis (DSA) to investigate the dynamic properties of HFBII adsorption layers on the air/water interface. This method is sensitive to the solidification of the surface layer and allows us to detect it and to investigate the dynamics of HFBII adsorption, the characteristic relaxation times upon interfacial expansion and compression, and to compare the values of the surface dilatational elasticity measured in different ways. Comparative experiments with Langmuir trough are carried out. The obtained results characterize the adsorption kinetics of HFBII hydrophobin; the mechanical properties of its interfacial layers, and their response to the action of external forces.

2. Materials and methods

2.1. Materials

The used protein, HFBII, is a class II hydrophobin isolated from the fungus *Trichoderma reesei* following the procedure described in Ref. [5]. A stock solution of concentration 0.0112 wt.% HFBII was prepared. All working solutions were prepared several hours before the measurements by dilution with either deionized water or aqueous solutions of NaCl. The HFBII solutions have a natural pH $\approx$ 6.3. The solutions with pH = 3.25 and pH = 7 were prepared using citric acid and NaOH, respectively. Because of the adhesive interactions between the hydrophobin molecules, their oligomeric aggregates in the aqueous phase stick to one another and aggregates of increasingly large size are formed. With time, this irreversible coagulations leads to the appearance of micrometer-sized aggregates that are visible by optical microscopy. However, by intensive sonication, the larger aggregates can be decomposed back to oligomers. Just before each measurement, the solution was sonicated in ultrasound bath for 5 min to break-up the formed aggregates. All solutions were prepared with deionized water of specific resistivity 18.2 MΩ cm (Milli-Q purification system). The working temperature was 25 °C.

2.2. Pendant-drop measurements

The interfacial layers from HFBII were investigated by means of two experimental methods: (i) the pendant drop method combined with drop-shape analysis (DSA), and (ii) Langmuir trough. The pendant drop measurements were carried out using the Contact-Angle-Drop-Shape-Analysis System 100 M (Krüss GmbH, Hamburg, Germany) with the DSA1 software. The drops were formed on the tip of a metal needle attached to a volume control system, which was a motor-driven syringe or a piezo-driven system. The method allowed us to measure the time dependence of the drop surface tension (as well as of drop volume and surface area) during various processes, e.g. relaxation after a disturbance or measurements in oscillatory regime. Detailed description of the used set-up and procedures can be found in Refs. [36,37].

2.3. Langmuir-trough measurements

A Langmuir trough with two barriers (Nima Technology Ltd., Coventry, UK) was used. The barriers moved symmetrically with a given linear speed. The subphase was pure water. Spread protein layers were formed by placing a drop from an aqueous HFBII solution on the water surface of area 150 cm^2 (between the barriers). The drops were of volume 600 μL from 0.012 wt.% HFBII solution, or 32.9 μL from 0.34 wt.% HFBII solution. The surface pressure was measured by means of a Wilhelmy plate made of chromatographic paper.

The spreading of aqueous drops in the Langmuir trough has the advantage that the water does not denature the protein. The disadvantage of this procedure is that the drop coalesces with the aqueous subphase, so that a part of the HFBII goes to the bulk, rather than to the interface. For this reason, the interfacial area per molecule is unknown in these experiments. The dependence of the surface pressure, π_s, on the total surface area between the barriers, A, was measured. The decrease of surface area was performed by a series of compression/relaxation steps, until A eventually reached a value of $\approx$50 cm^2. Next, a similar stepwise expansion back to A = 150 cm^2 was carried out. Each compression (or expansion) step consisted of area change with 5 cm^2 at 10 cm^2/min barrier translation speed, followed by relaxation for 2.5 min at rest. After that, the next step was performed. This experimental protocol was chosen because of the slow relaxation of the protein layer. After each compression (or expansion) step, the surface pressure π_s relaxed during the subsequent 2.5 min of waiting. The value of π_s at the end of relaxation can be considered as the equilibrium value of π_s at the respective A. In this way, an equilibrium π_s-vs.-A isotherm can be obtained.

In addition, at each step the experimental surface-pressure variation, $\Delta\pi_s$, corresponding to an area variation, ΔA, allowed us to determine the value of surface dilatational elasticity, E, as a function of the equilibrium π_s, measured just before the area variation, ΔA. Experimental data are presented in the next sections.

3. Fluid vs. elastic protein surface layers

The experiment [4] shows that HFBII forms elastic surface layers (membranes) at the air/water interface, which have non-zero surface shear elasticity, $E_{sh} > 0$. However, at sufficiently low surface concentrations, the HFBII interfacial layer is expected to be fluid ($E_{sh} = 0$). Then, a transition from fluid to solid (elastic) interfacial layer is expected with the rise of HFBII surface concentration. Here,

for brevity this phase transition will be termed "solidification" of the adsorption layer.

Experimentally, the phase transition can be detected during the pendant-drop + DSA experiments as follows. Because of the adsorption of HFBII from the drop interior, the surface tension decreases and the drop profile becomes increasingly elongated (Fig. 1). The used apparatus records video frames of the pendant drop every 40 ms. After the experiment, these video frames have been automatically processed by fitting the drop profile with the Laplace equation of capillarity. The fit yields the surface tension, surface area, and the drop volume for each frame. The error of the fit, characterizing the difference between the experimental and Laplace profiles, is also registered.

As illustration, in Fig. 1 the error of the Laplace fit is plotted vs. the determined surface tension, σ. The data show that for $\sigma < 50$ mN/m, the error of the fit exhibits a steep increase, which indicates that the experimental profile does not obey the Laplace equation. This deviation can be explained with solidification of the HFBII adsorption layer. Indeed, the surface tension of a solidified (elastic) adsorption layer is a non-isotropic (tensorial) quantity, whereas the conventional Laplace equation holds for an interface with isotropic (scalar) tension; see e.g. [38–40].

In other words, the pendant-drop + DSA experiments indicate a surface phase transition at $\sigma \approx 50$ mN/m, which corresponds to surface pressure $\pi_s = 72 - \sigma \approx 22$ mN/m (Fig. 1). It is remarkable that the DSA method, which is usually applied to measure *dilatational* surface rheology [28], can detect also the effect of surface solidification, i.e. the appearance of surface *shear* elasticity, E_{sh}, through the deviations from the Laplace shape.

The experiments in the Langmuir trough also indicate the existence of surface phase transition. It appears as a flat (or less steep) region in the π_s-vs.-A isotherm (Fig. 2), which again corresponds to $\pi_s \approx 22$ mN/m, as the transition in Fig. 1. The mean value of the surface pressure at the phase transition, obtained by averaging over 20 experiments, is $\pi_s = 22 \pm 4$ mN/m. A yielding of the protein layer at about $\pi_s \approx 20$ mN/m was observed also in the Langmuir-trough experiments in Ref. [4].

Fig. 3 shows the relaxation of the surface tension of pendant drops from HFBII solutions after the drop formation. As expected, σ decreases with time because of the increasing adsorption of protein. This decrease is faster at the higher protein concentrations owing to the more intensive supply of protein from the bulk. At 0.001 wt.% HFBII, σ decreases very slowly indicating a slow HFBII adsorption. The addition of 100 mM NaCl does not accelerate the adsorption at pH = 7. However, at pH = 3.25 the adsorption becomes faster. The latter fact can be attributed to electrostatic attraction between the negatively charged air/water interface [41–44] and the hydrophobin aggregates, which are positively charged at pH = 3.25 [5,45]. In contrast, pH = 7 is close to the HFBII isoelectric point, where such electrostatic attraction is absent.

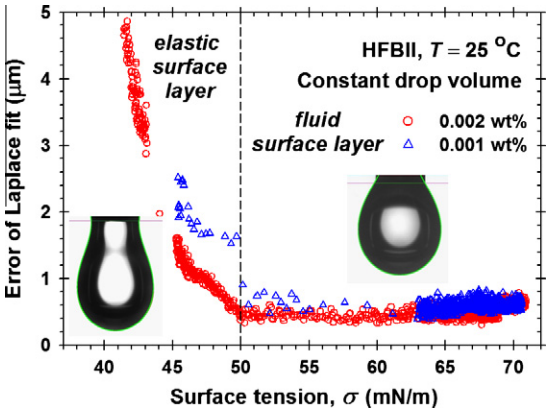

Fig. 1. Plot of the error of the fit of the drop profile by means of the Laplace equation vs. the surface tension, σ, determined by the pendant drop method + DSA at two HFBII concentrations. The used apparatus automatically calculates the error of the fit. Its greater values at smaller σ indicate deviations from the Laplace shape due to solidification of the adsorption layer. The left and right photographs correspond to $\sigma = 41.2$ and 65.2 mN/m.

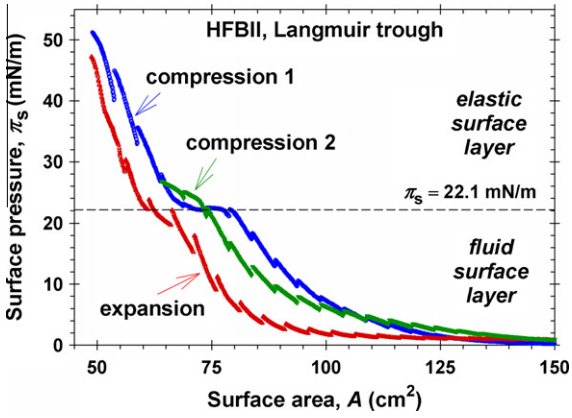

Fig. 2. Surface pressure, π_s, vs. surface area, A, measured by a Langmuir trough. The interfacial layer is formed by spreading 600 μL of 0.012 wt.% aqueous solution of HFBII on 150 cm^2 of the surface of pure water in the trough. The three curves correspond to consecutive compression, expansion, and second compression of the same layer.

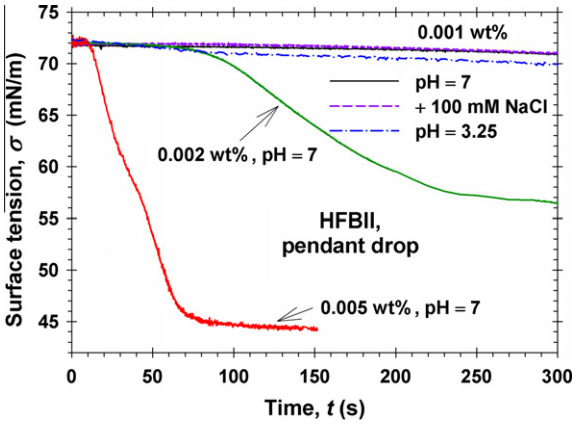

Fig. 3. Dynamic surface tension, σ, vs. time t, measured with the pendant drop method + DSA for HFBII solutions of different concentrations, denoted in the figure, at different pH.

Fig. 3 shows also that at 0.002 wt.% HFBII, the surface tension levels off at $\sigma \approx 56$ mN/m, whereas at 0.005 wt.% σ tends to a constant value of ≈44 mN/m. The latter value is <50 mN/m ($\pi_s > 22$ mN/m), and in view of the results in Figs. 1 and 2 the lower part of the surface tension isotherm at 0.005 wt.% HFBII (Fig. 3) belongs to the region of elastic surface layers. In this region, the error of the Laplace fit is relatively large (Fig. 1), so that the respective values of σ given by the DSA apparatus are not reliable. Hence, at 0.005 wt.% HFBII (and at higher concentrations), the pendant drop + DSA method does not give correctly the equilibrium σ values. For this reason, all our subsequent DSA measurements have been carried out at lower concentrations, viz. 0.001 and 0.002 wt.% HFBII, at which the adsorption layer is fluid (non-solidified). The portions of the experimental curves with $\sigma < 50$ mN/m, like the lowest curve in Fig. 3, present only the values displayed by the DSA apparatus, but these values do not express the conventional isotropic surface tension.

The time needed for solidification of the adsorption layer depends strongly on the hydrophobin concentration. As seen in

Fig. 3, at 0.005 wt.% HFBII σ reaches 50 mN/m (the layer solidifies) for ≈1 min, whereas the experiment shows that at 0.002 wt.% HFBII the adsorption layer solidifies after 10 min.

In summary, our experiments by both pendant drops and Langmuir trough showed that the solidification of the HFBII adsorption layers on water happens at $\pi_s \approx 22 \pm 4$ mN/m. Experiments by Langmuir trough [4,46] indicated that the buckling of the HFBII layers occurs at $\pi_s = 50$–60 mN/m. We could hypothesize that in the intermediate range of surface pressures, $22 < \pi_s < 50$ (mN/m), the slow compression of the HFBII layer leads to filling of the numerous voids that have been observed [3,47,48] in the solidified (viscoelastic) hydrophobin adsorption layers.

4. Interfacial relaxation times

4.1. Experiments with buoyant bubbles

We carried out experiments not only with pendant drops, but also with buoyant bubbles attached to the tip of a capillary. The profile of the buoyant bubbles is similar to that of the pendant drops (rotated at 180°), so that the surface tension and area can be determined from the bubble profile by using the DSA apparatus.

Fig. 4a shows results for a buoyant bubble, which is initially formed in a 0.001 wt.% HFBII solution of volume 20 mL and equilibrated for 18 min, so that the surface tension becomes $\sigma \approx 55$ mN/m. The goal of the experiment is to exchange the HFBII solution with pure water and to check whether the adsorbed protein will desorb from the bubble surface. For this goal, two similar peristaltic pumps of flow rate 10 mL/min have been used. The first pump supplies pure water, whereas the second one pumps out the aqueous phase. For the 30 min period of "washing" (Fig. 4a), the volume of the injected pure water is 300 mL, i.e. 15 times the volume of the experimental cell. Having in mind the low initial HFBII concentration, after such a dilution the bubble is practically surrounded by pure water. However, Fig. 4a shows that the exchange of the protein solution with pure water does not lead to any essential changes in the surface tension, σ. Some small variations in σ are due to fluctuation of the bubble area, as seen in the figure. Finally, the bubble has been subjected to an expansion and a compression. The corresponding variations of the surface tension correspond to the behavior of an insoluble surface layer. This experiment indicates that having once adsorbed at the air/water interface, HFBII does not desorb, even in pure water. In other words, the adsorption of HFBII at the air/water interface is *irreversible*. Hence, the adsorption energy of HFBII is much greater than the adsorption energy of the conventional surfactants.

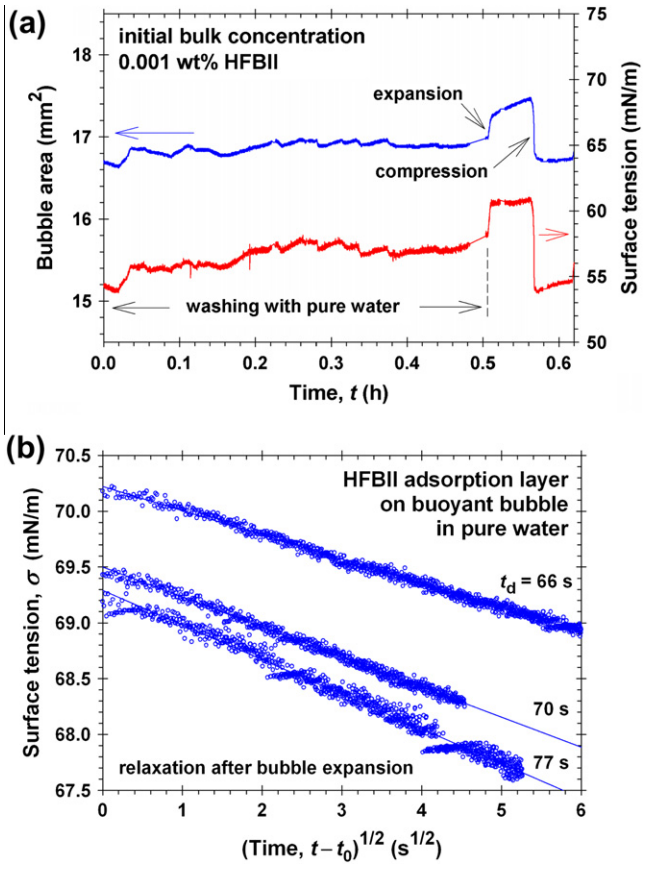

Fig. 4. Experiments with buoyant bubbles. (a) Variation of the surface tension and area for a bubble, initially formed formed in a 0.001 wt.% HFBII solution, during the exchange of the aqueous phase with pure water at $0 \leq t \leq 0.5$ h. (b) Relaxation of the surface tension of buoyant bubbles covered by HFBII adsorption layers in pure water after an initial fast expansion; the characteristic relaxation time, t_d, is shown at each curve; see Eq. (1).

After the end of such an experiment, the bubble is detached and a new bubble is formed. The latter has surface tension ≈72 mN/m, which confirms that the ambient aqueous phase is pure water.

In another series of experiments, after exchanging the protein solution with pure water, the bubble covered with an HFBII adsorption layer was quickly expanded and the relaxation of its surface tension was recorded. During this experiment, the bubble surface area was kept constant. As seen in Fig. 4b, the relaxation follows a square-root law, which corresponds to the early stage of surface-tension relaxation under diffusion control after a small perturbation [49–51]:

$$\frac{\sigma(t) - \sigma_{eq}}{\sigma_0 - \sigma_{eq}} = 1 \pm \frac{2}{\sqrt{\pi}} \sqrt{\frac{t - t_0}{t_d}} \tag{1}$$

The sign is '+' or '−' for relaxation after compression and expansion, respectively; t_0 is the moment of the compression/expansion; t_d is the characteristic time of relaxation under diffusion control; σ_0 is the value of surface tension just after the perturbation; σ_{eq} is the equilibrium surface tension. To estimate t_d from the slopes of the experimental curves, we set σ_{eq} equal to the surface tension just before the perturbation; σ_0 was determined from the intercepts of the fits of the experimental curves. The values of t_d estimated in this way vary in the range $66 \leqslant t_d \leqslant 77$ s for the lines in Fig. 4b.

In the case of conventional surfactants, Eq. (1) with sign '−' describes the decrease of surface tension of an initially expanded interface because of the supply of new surfactant molecules from the bulk of solution. However, in the present case (Fig. 4b) the aqueous phase is pure water. In such a case, the relaxation of σ can be explained with a surface-diffusion-controlled release of protein molecules from surface aggregates; see Fig. 5b. A similar mechanism was observed with bovine serum albumin (BSA) at the oil/water interface [52]. A more detailed discussion is given in Section 4.2.

4.2. HFBII layers spread on pure water in Langmuir trough

The above results for buoyant bubbles are helpful for understanding the kinetics of σ in the Langmuir trough, where a HFBII layer is spread on pure water. Such layers were quickly expanded, and after that σ slowly relaxed (decreased) following a square-root law (Fig. 5a). In other experiments, the layers were quickly compressed, and after that σ slowly increased following again a square-root law (Fig. 5a). As already mentioned, the latter law indicates diffusion-controlled kinetics at early times; see e.g. Refs. [49–51]. Insofar as the adsorption of HFBII is irreversible and the

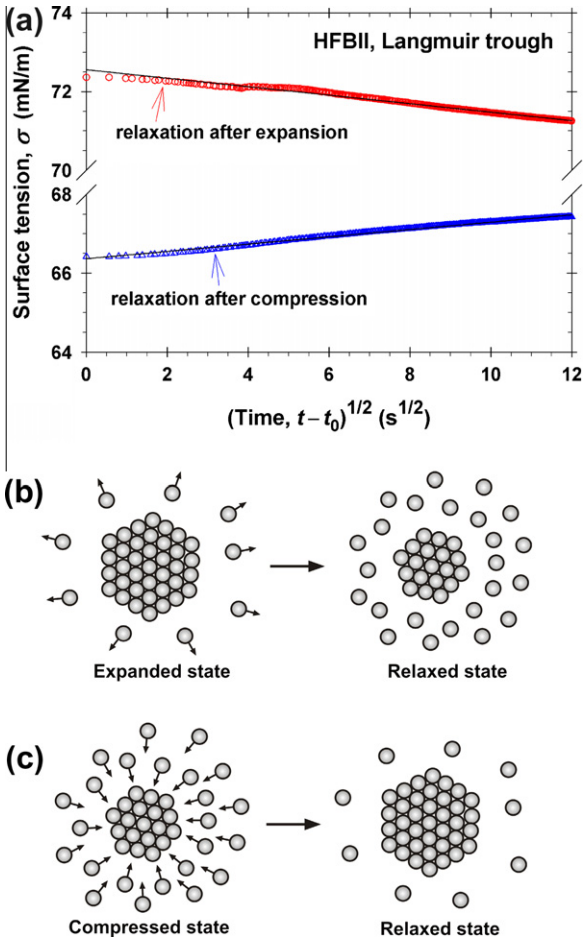

Fig. 5. (a) Experimental dependence of the surface tension on the square root of time measured in a Langmuir trough after an initial expansion (or compression) of an HFBII layer spread on the surface of pure water. (b) After the initial expansion, protein molecules are detaching from a surface aggregate to saturate the surrounding diluted surface phase. (c) After the initial compression, protein molecules are condensing on the aggregates to attain equilibrium between the aggregates and the surrounding diluted surface phase.

subphase in the Langmuir trough is pure water, the diffusion-controlled kinetics can be only due to the detachment/ attachment of HFBII molecules from 2D protein aggregates at the air/water interface. Upon expansion, such aggregates can release HFBII molecules to saturate the diluted surface phase around it (Fig. 5b). Upon compression, the monomeric HFBII molecules can condense on the periphery of the aggregates (Fig. 5c). These processes of release and condensation can happen under surface-diffusion control [52], which is the most probable explanation of the observed square-root law in Figs. 4b and 5a.

For reversible processes, the relaxation times after compression and expansion must be the same. However, the processes with the 'sticky' hydrophobin molecules are strongly irreversible, as seen from the surface pressure isotherms in Fig. 2. The reason is that upon compression and expansion the hydrophobin adsorption layers undergo structural changes including merging and splitting of surface aggregates, as well as appearance and disappearance of voids in the surface layer; see Section 5 for additional data and discussion.

4.3. Expansion/relaxation and compression/relaxation cycles with pendant drops

The characteristic interfacial relaxation times of fluid HFBII adsorption layers were determined in DSA experiments with pendant drops like those illustrated in Fig. 6; see also Ref. [53]. The working concentrations were 0.001 and 0.002 wt.% HFBII to be sure that the DSA method works properly ($\sigma > 50$ mN/m); see the upper curves in Fig. 3. After a relaxation for about 30 min, the volume of the pendant drop was increased which leads to a fast expansion of the adsorption layer, followed by a new relaxation process (Fig. 6). Next, the layer was compressed (by decreasing the drop volume) and the relaxation of σ after compression was recorded.

Further, the cycle of expansion/relaxation and compression/relaxation was repeated. After the second compression, the adsorption layer solidified, which was indicated by a rise in the error of the Laplace fit and by the appearance of wrinkles at the neck of the pendant drop (Fig. 6). It should be noted that during all relaxation stages, the volume of the drop was kept constant.

4.4. Relaxation of the surface tension of pendant drops after expansion

Experimental curves of surface-tension relaxation after an interfacial expansion are shown in Fig. 7a for experiments carried out with the pendant-drop method. The data analysis indicates that the relaxation after expansion follows an exponential-decay law:

$$\frac{\sigma - \sigma_{eq}}{\sigma_0 - \sigma_{eq}} = \exp\left(-\frac{t - t_0}{t_r}\right) \tag{2}$$

Here, σ_0 and t_0 are the experimental surface tension and moment-in-time corresponding to the beginning of relaxation; t_r is the characteristic relaxation time, and σ_{eq} is the equilibrium surface tension (at $t \to \infty$). σ_0 and t_0 and are known from the experiment, whereas σ_{eq} and t_r have been determined from the fits as adjustable parameters. In Fig. 7b, the obtained values are plotted as t_r vs. σ_{eq}. The plots show that the relaxation is slower (t_r is greater) at pH = 3.25, in comparison with pH = 7, at the same HFBII concentration (0.002 wt.%). At the lower HFBII concentration (0.001 wt.%), the relaxation is even slower (Fig. 7b).

The exponential decay of the surface tension upon relaxation indicates adsorption kinetics under barrier control [51,54]. Conversely, the experiments with HFBII layers on the surface of pure water (Figs. 4b and 5a) show that the release/attachment of protein molecules from/to surface protein aggregates occurs under surface-diffusion control (Fig. 5b and c). In the present case (Fig. 7a), the main difference is that the aqueous phase is a protein solution,

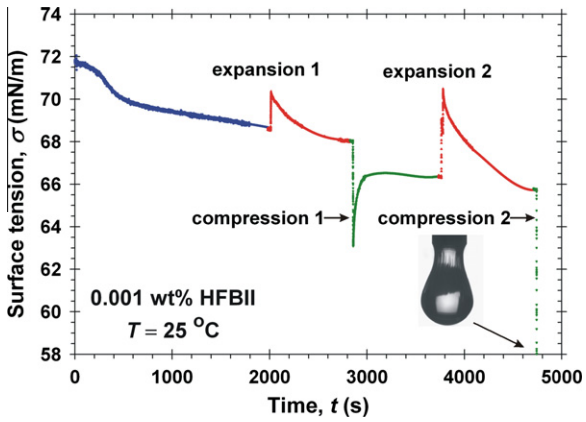

Fig. 6. Surface tension, σ, vs. time, t, experimental curve measured by the pendant drop method + DSA. By varying the volume of the drop, the HFBII adsorption layer has been subjected to consecutive cycles of fast expansion–relaxation, and fast compression–relaxation. After the second compression, the adsorption layer has undergone a transition to elastic film (skin), as indicated by the appearance of wrinkles in the zone of the drop's neck.

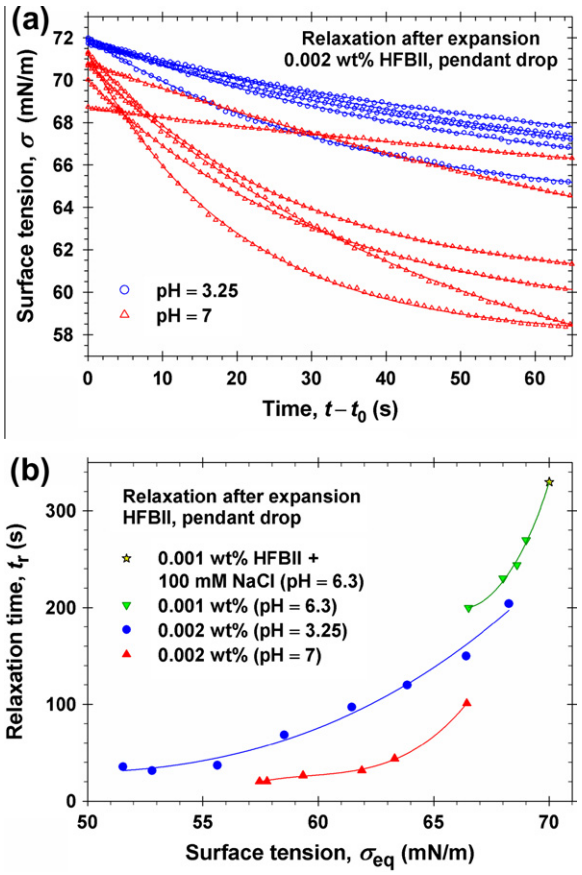

Fig. 7. Surface tension relaxation after a fast expansion of the interface: (a) Experimental data for surface tension vs. time for the relaxation of surface tension after a fast initial expansion that was performed at the moment $t = t_0$; the lines represent the best fits with an exponential-decay function, Eq. (2). (b) Plot of the relaxation time, t_r, vs. the equilibrium surface tension, σ_{eq}, both of them determined from the fits; the lines are guides to the eye. The HFBII concentrations and the pH values are denoted in the figure.

rather than pure water. So, the different adsorption kinetics can be explained with a predominant adsorption of HFBII molecules from the bulk. "Barrier control" means that among the two consecutive processes, viz. transfer of protein (i) from the bulk to the subsurface by diffusion and (ii) from the subsurface to the surface, the second process is much slower because of the presence of a kinetic barrier to adsorption.

In the considered concentration range, HFBII exists in the bulk in the form of oligomeric aggregates, mostly tetramers [8–11]. Hence, the adsorption of a HFBII molecule includes a stage of its detachment from an aggregate [55,56], which could be the main reason for the barrier to adsorption at pH between 6 and 7 (near the isoelectric point of HFBII). At pH = 3.25, the HFBII molecules (and aggregates) and the adsorption layer at the interface are positively charged so that the electrostatic repulsion gives an additional contribution to the adsorption barrier [57], which can explain the greater t_r at the lower pH. The slowest adsorption (the greatest t_r) at 0.001 wt.% HFBII can be due to the fact that the relaxation time increases with the decrease of the protein bulk concentration in the case of barrier control [51].

Adsorption under barrier control has been observed also with other proteins, e.g. with BSA structural intermediates [58] and with Na caseinate [59]. It is worthwhile mentioning that the Na caseinate also forms aggregates (caseinate micelles) in the bulk of solution [60].

Another contribution to the barrier to HFBII adsorption could originate from the steric hindrance by protein molecules that have already adsorbed at the interface. Note, however, that a steric barrier could hardly explain the increase of t_r with the rise of σ_{eq} at a fixed protein concentration (Fig. 7b). Indeed, at a higher surface tension the surface coverage should be lower so that the steric hindrance and t_r should decrease with the rise of σ_{eq}. However, exactly the opposite tendency is experimentally observed (Fig. 7b): the greater the surface coverage, the faster the adsorption. The situation is similar in the case of pH = 3.25, where electrostatic contribution to the adsorption barrier is also expected: At the greater σ_{eq} the surface coverage and electric potential should be lower, so that t_r should decrease, in contrast with the experimental tendency. A possible explanation of the observed dependence of t_r on σ_{eq} (Fig. 7b) can be given if the hydrophobic attraction between the HFBII molecules [12] is taken into account. When the surface coverage increases (σ_{eq} decreases) the hydrophobic attraction should increase and lower the adsorption barrier, which in its own turn would accelerate the adsorption and lead to smaller t_r, in agreement with the experimental findings.

It should be noted that unlike the surface-tension measurements, the ellipsometric measurements of adsorbed mass are insensitive to the investigated interfacial relaxation processes. In the case of barrier-limited adsorption kinetics, the relaxation represents transfer of protein molecules from the subsurface to the surface, but the ellipsometry gives the total amount at the surface + subsurface. Moreover, the ellipsometry registers the average mass per unit area of a macroscopic spot on the surface, so that it cannot detect the effect of surface-diffusion-limited exchange of protein molecules between microscopic surface aggregates and the surrounding interface (Fig. 5b and c).

4.5. Relaxation of the surface tension of pendant drops after compression

Fig. 8a shows relaxation curves (pendant-drop-DSA method) representing plots of the variation of surface tension, σ, after an interfacial compression plotted vs. the square root of time. The plots represent straight lines, which indicates that the relaxation of σ occurs under diffusion control. A possible physical mechanism can be that sketched in Fig. 5c. Indeed, as mentioned above, the adsorption of HFBII at the air/water interface is irreversible, so that desorption of HFBII molecules upon compression is not expected. In such a case, the only possible mechanism of surface relaxation can be a two-dimensional (surface) process, like condensation of HFBII monomers at the periphery of surface aggregates as illustrated in Fig. 5c. The picture in the latter figure is simplified: in reality, the diluted phase can contain not only HFBII monomers, but also oligomeric aggregates of this protein.

We can estimate the characteristic relaxation time after a surface compression using Eq. (1). The obtained values of t_d vary in the range $83 \leqslant t_d \leqslant 219$ s for the curves in Fig. 8a. These t_d values are of the same order of magnitude as t_r in Fig. 7b, despite the fact that t_d and t_r characterize different kinetic regimes: diffusion vs. barrier control.

In general, the relaxation times depend on the surface concentration and can vary in a wide range. For example, using Eq. (1) for the two lines in Fig. 5a (Langmuir trough) we determine $t_d = 82$ and 89 min for the relaxation after compression and expansion, respectively. The latter values are about 34 times greater than the mean relaxation time in Fig. 8a, which can be attributed to a lower surface density of HFBII in these specific Langmuir-trough experiments, as indicated by the higher σ values in Fig. 5a.

If the surface compression is large enough, the protein layer can solidify and then no relaxation of σ is detected, see Fig. 8b. In the latter figure, after the compression σ does not increase with time (as in Fig. 8a) but remains almost constant. The error of the Laplace fit of the drop profile strongly increases after the compression

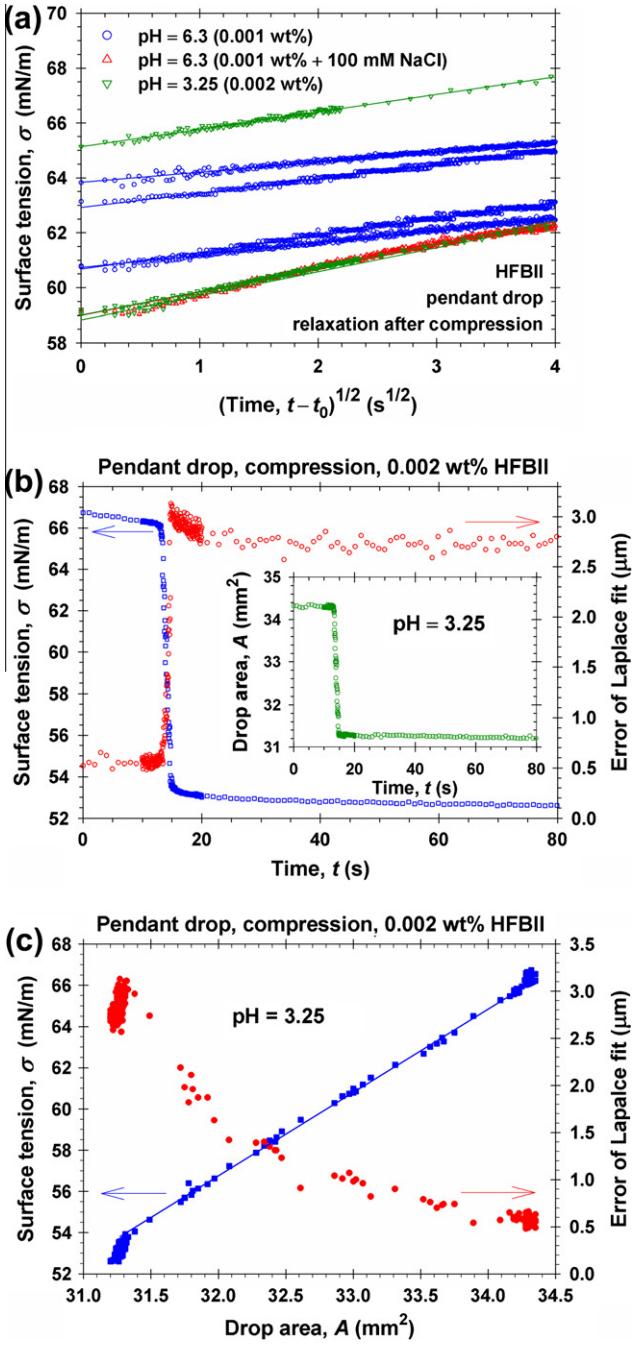

Fig. 8. (a) Surface tension relaxations after an initial interfacial compression – the surface tension grows linearly with the square root of time. (b) After a fast compression, σ does not relax (remains almost constant), which indicates surface solidification upon compression in the considered experiment. (c) Plot of the data from panel b as σ vs. A; the error of the Laplace fit of the drop profile is also shown (see Fig. 1).

(Fig. 8b), which is an indication for the solidification of the adsorption layer.

5. Dilatational surface elasticity

5.1. Definition and experimental data

The standard definition of dilatational surface elasticity, due to Gibbs [61], is:

$$E \equiv A\frac{\partial\sigma}{\partial A} = \frac{\partial\sigma}{\partial\alpha} \tag{3}$$

where α is the surface dilatation:

$$\alpha \equiv \ln\left(\frac{A}{A_0}\right) \tag{4}$$

A_0 is the initial surface area, in the beginning of dilatation; $\alpha > 0$ for expansion, whereas $\alpha < 0$ for compression. The definition given by Eq. (3) is strict for insoluble surfactants, whereas for soluble surfactants, the dilatation must be much faster that the characteristic rate of surfactant exchange between the surface and the adjacent bulk phases (adsorption/desorption).

At small area variations, $\Delta A \ll A_0$, from Eqs. (3) and (4) we obtain:

$$\alpha = \ln\left(\frac{A_0 + \Delta A}{A_0}\right) \approx \frac{\Delta A}{A_0} = \frac{A - A_0}{A_0} \tag{5}$$

$$\Delta\sigma \approx \frac{\partial\sigma}{\partial A}\Delta A = A\frac{\partial\sigma}{\partial A}\frac{\Delta A}{A} \approx E\alpha \tag{6}$$

An example for fast surface compression is given in Fig. 8b – see the steep parts of the experimental $\sigma(t)$ and $A(t)$ dependencies. In Fig. 8c, σ is plotted vs. A for the experimental points corresponding to the region of fast compression in Fig. 8b. The obtained σ-vs.-A dependence is linear; from its slope the elasticity E can be determined in accordance with Eqs. (5) and (6). It is interesting to note that the dependence in Fig. 8c is linear even in the region of larger errors of the Laplace fit (shown in the same figure), where the values of σ (determined by DSA) are expected to be influenced by the solidification of the surface layer.

Fig. 9a shows the variation of surface tension, $\Delta\sigma$, upon expansion of a pendant drop, plotted vs. the surface dilatation, α, at pH = 6.3 and 7, i.e. close to the isoelectric point of HFBII [5,45]. Each experimental curve corresponds to a given value of the surface pressure, π_{s0}, measured just before the surface dilatation. The data comply very well with straight lines, in accordance with Eq. (6). Their slopes yield the values of the surface elasticity E. The slopes (and E) grow with the rise of the initial surface pressure, π_{s0}.

Fig. 9b and c shows similar data for $\Delta\sigma$ vs. α, but this time the surface dilatation is carried out with HFBII layer spread on pure water in the Langmuir trough (rather than with pendant drops). In this case, pH ≈ 6 is that of the aqueous subphase. Fig. 9b corresponds to expansion, whereas Fig. 8c corresponds to compression. In both cases, the plots of $\Delta\sigma$ vs. α agree very well with straight lines, whose slopes depend on the initial surface pressure, π_{s0}.

5.2. Results for the surface elasticity and discussion

The values of the surface dilatational elasticity, E, determined from the slopes of $\Delta\sigma$ vs. α plots, including those in Figs. 8c and 9, are summarized in Fig. 10. The data at $6 \leqslant$ pH $\leqslant 7$ in Fig. 10a show that for $\pi_{s0} < 11$ mN/m close values of E are obtained in compression and expansion experiments, with both pendant drops and Langmuir trough. The values of the surface dilatational storage modulus, E', determined in oscillatory experiments (Section 6) are also close to the E values obtained in the compression of expansion experiments. (As a rule, $E' \approx E$ for oscillatory periods that are much smaller than the characteristic relaxation time.)

In contrast, for $\pi_{s0} > 11$ mN/m the data for E are scattered (Fig. 10a). A tendency for E to decrease with the rise of π_{s0} is observed, which is more pronounced (appears at lower π_{s0}) for the compression experiments. The same tendency (increase of E at the lower π_{s0}, but decrease of E at the higher π_{s0}) is clearly seen for the HFBII data in Fig. 10b, which have been obtained at

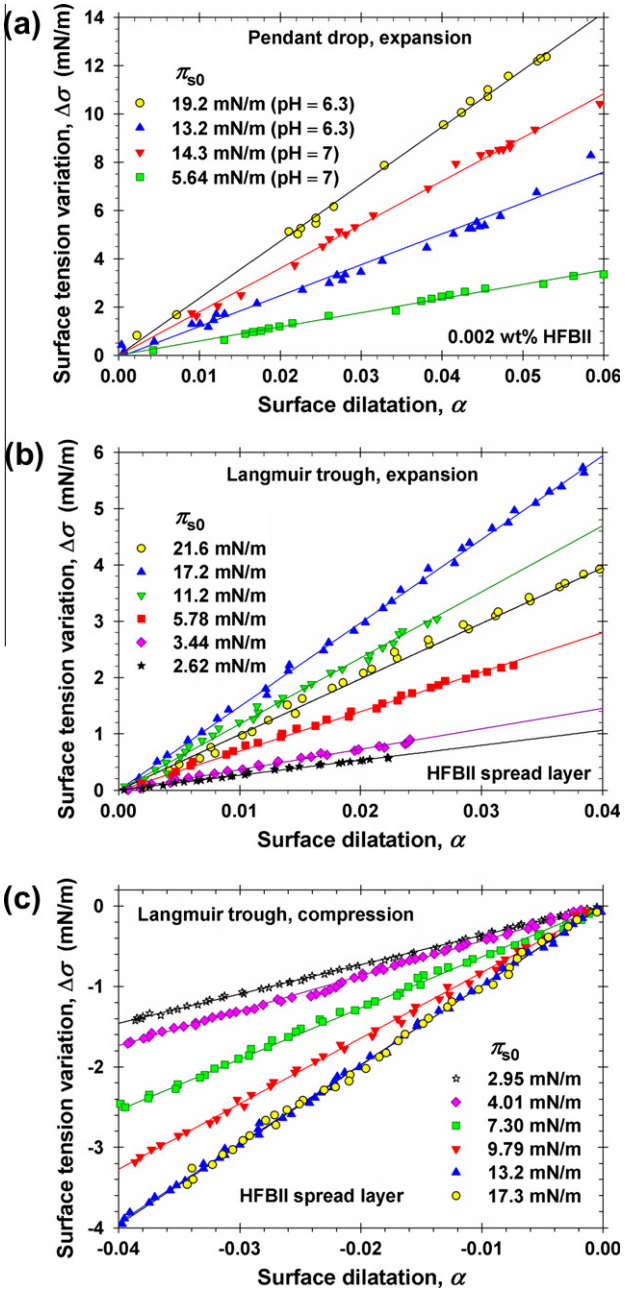

Fig. 9. Plots of experimental data for the surface tension variation, $\Delta\sigma = \sigma(t) - \sigma(t_0)$, vs. the surface dilatation, $\alpha \equiv \ln[A(t)/A(t_0)]$, where A is the surface area; t_0 is the initial moment of dilatation, and π_{s0} is the value of surface pressure just before the dilatation. (a) Interfacial expansion of a pendant-drop. (b) Interfacial expansion in a Langmuir trough. (c) Interfacial compression in a Langmuir trough; the negative α means shrinking of the surface area, $A(t) < A(t_0)$.

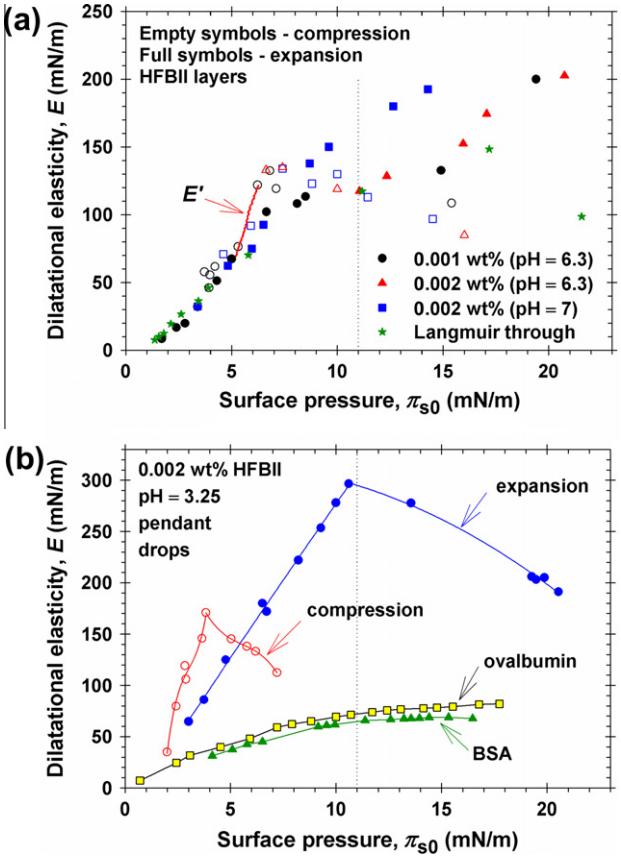

Fig. 10. Plots of the surface dilatational elasticity, E, vs. π_{s0} determined from the slopes of lines like those in Fig. 9, each of them corresponding to a given π_{s0}. (a) Data at pH = 6.3 and 7. For the experiments with pendant drops, the full and empty symbols with the same shape correspond to expansion and compression at the same HFBII concentration denoted in the figure. The experiment in the Langmuir trough is performed with a HFBII layer spread on pure water. The solid segment represents the data for E' vs. π_s from Fig. 11b obtained with an oscillating pendant drop. (b) Data for HFBII at pH = 3.25 are compared with data for ovalbumin and BSA from Ref. [31]. The lines are guides to the eye.

pH = 3.25. At this lower pH, greater values of E are measured in comparison with the results at pH = 6–7 in Fig. 10a. Differences between the E-vs.-π_{s0} dependences obtained upon expansion and compression have been observed also in Ref. [4] at $\pi_{s0} >$ 11–14 mN/m, in Langmuir-trough experiments.

The increasing branch of the E-vs.-π_{s0} dependence (at the lower π_{s0}) can be explained with the higher surface concentration of adsorbed HFBII monomers (and oligomers) that give rise to greater π_{s0} and E values. At pH = 3.25, the electrostatic repulsion between the charged HFBII monomers contributes to the surface elasticity [62,63] and, moreover, leads to the formation of more monomers and less oligomers, which could explain the greater values of E for HFBII in Fig. 10b as compared with Fig. 10a. Fig. 10b illustrates also the greater dilatational elasticity of the HFBII adsorption layers at the air/water interface in comparison with analogous data from [31] for other proteins: BSA and ovalbumin.

For $\pi_{s0} > 11$ mN/m, the data are scattered (Fig. 10a) and some of the experimental curves exhibit a maximum. Similar maxima in the E-vs.-π_s curves have been observed with other globular proteins, such as bovine serum albumin (BSA), ovalbumin and β-lactoglobulin at both air/water and oil/water interfaces [26,27,31,34]. In our case, the maxima cannot be explained with shrinking of the interfacial area occupied by an adsorbed protein molecule upon compression, insofar as the HFBII molecules are not expected to undergo conformational changes at the interface (see Section 1).

A possible explanation of the layer's behavior at the higher surface pressures could be the following. The lateral hydrophobic attraction [12] between the adsorbed HFBII molecules and oligomers can lead to the formation of surface aggregates from hydrophobin, as sketched in Fig. 5b and c. The surface aggregation can explain the scattering of the data for $\pi_{s0} > 11$ mN/m in Fig. 10a and the decreasing branches of the E-vs.-π_{s0} plots in Fig. 10b. The aggregation is promoted by the surface compression (Fig. 8b), which explains why the deviations from the increasing branch of the E-vs.-π_{s0} dependence happen easier upon compression in comparison with expansion (Fig. 10a and b). The smaller E values at $\pi_{s0} > 11$ mN/m can be physically explained with the fact that upon compression (expansion), HFBII monomers and oligomers attach to (detach from) the aggregates, which leads

to smaller variations in the surface concentration of monomers and oligomers in the diluted phase.

Another point that deserves discussion is why the change in the trend of surface elasticity (Fig. 10) occurs at about $\pi_s \approx 11$ mN/m, whereas the solidification of the adsorption layer happens at a higher surface pressure, viz. $\pi_s \approx 22$ mN/m; see Fig. 1 and 2. We could hypothesize that the transition in elasticity at $\pi_s \approx 11$ mN/m (Fig. 10) occurs at the appearance of isolated spots of the condensed surface phase dispersed in the diluted surface phase. In contrast, the interfacial solidification at $\pi_s \approx 22$ mN/m (Figs. 1 and 2) happens at a greater degree of surface coverage, at which the spots are in contact with each other, coalesce and form a continuous elastic network, which might contain dispersed voids (percolation threshold). This hypothesis will be verified in subsequent experiments.

6. Experiments with oscillating pendant drops

A representative set of data is shown in Fig. 11. The volume of the pendant drop is subjected to regular sinusoidal oscillations of period 5 s. The surface tension, σ, determined from the drop profile also exhibits oscillations, but their amplitude gradually increases with time, t, whereas the mean value of σ slightly decreases (Fig. 11a). The experimental time dependence of the area, $A(t)$, is practically a regular sinusoid with a weak tendency of the mean value of A to decrease.

Because the drop contains 0.002 wt.% HFBII, during the expansion of its surface new protein molecules can adsorb. However, they are not expected to desorb during the interfacial compression insofar as the adsorption of hydrophobin is irreversible (see Section 4.1). In this way, the oscillations in the drop surface area lead to a "pumping" of the surface with HFBII molecules and to a corresponding increase in the amplitude of oscillations. The effect of "pumping" on the average surface pressure is not so large: π_s increases from 5.2 to 6.3 mN/m (see the horizontal axis in Fig. 11b), which corresponds to the decrease of the mean value of σ in Fig. 11a. However, this small increase of π_s leads to a considerable increase of the surface dilatational storage modulus, E', from 70 to 120 mN/m; see Fig. 11b.

By definition, the storage and loss surface dilatational moduli, E' and E'', represent the real and imaginary parts of the surface elasticity [64]:

$$\frac{\partial \sigma}{\partial \alpha} = E'(\omega) + iE''(\omega) \tag{7}$$

In general, both E' and E'' depend on the angular frequency, ω [33,64–66]. The data in Fig. 11b are obtained at a fixed frequency, but at different surface pressures.

Because the σ-vs.-t and A-vs.-t dependences in Fig. 11a are not regular sinusoids, the data were processed by sliding Fourier analysis, as follows. The experimental points contained in a "window" of width equal to one period were fitted with sinusoid, and the values of E' and E'' were calculated for this position of the window. (One period of 5 s contains 120 experimental points.) Then, the "window" was shifted with a step of 0.2 s to the right, and the values of E' and E'' were calculated for the new position of the "window". The shift of the "window", and the related calculations, were repeated many times until reaching the end of the experimental curve.

The obtained values of E' and E'' are plotted in Fig. 11b vs. the corresponding surface pressure. The results show that $E' \gg E''$, which means that the rheological response of the HFBII adsorption layer upon dilatation is predominantly elastic. As already mentioned, the values of E' obtained in our oscillatory experiments at a period of 5 s are close to those of E obtained in expansion and compression experiments (Fig. 10a).

Similar oscillatory experiments with pendant drops gave E' from 77 to 86 mN/m for β-lactoglobulin [28] vs. E' from 70 to 120 mN/m for HFBII in our experiments. In other words, HFBII exhibits a greater surface elasticity, as expected. In contrast, the values of the loss modulus are close for the two different proteins: E'' varies from 13 to 16 mN/m for β-lactoglobulin [28], whereas E'' varies from 5 to 13 mN/m for HFBII in our experiments. For these proteins, E'' can be attributed to the true friction in the adsorption layer rather than to an apparent viscosity originating from the diffusion exchange of molecules between the interface and the adjacent liquid phase, as it is for low-molecular surfactants [67]. In addition, the experiments were carried out with a sufficiently wide capillary (of 1.54 mm inner diameter) to be sure that the effect of the bulk viscous dissipation on the measured loss modulus is negligible; for details see Ref. [37].

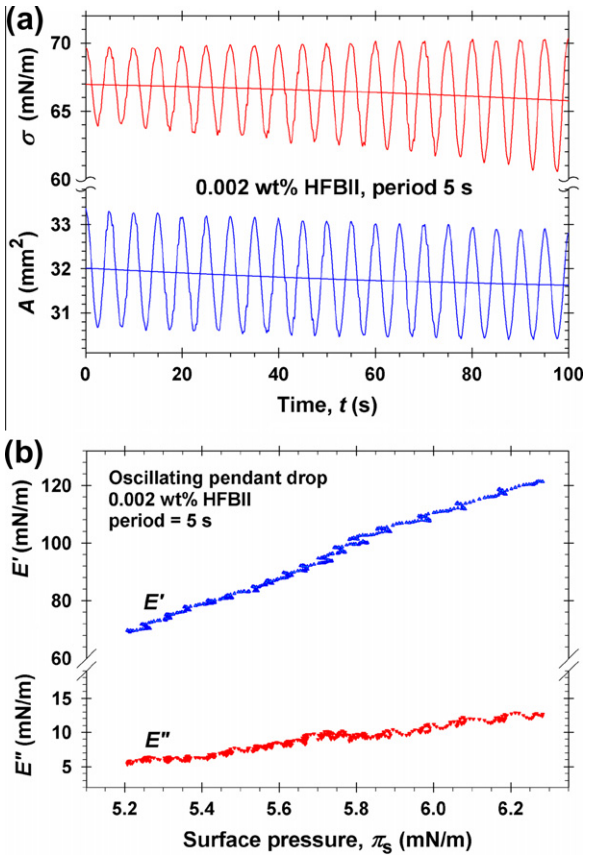

Fig. 11. Experimental data for an oscillating (period 5 s) pendant drop from 0.002 wt.% HFBII solution at pH = 6.3. (a) A vs. t and σ vs. t are the time dependences of drop surface area and surface tension, respectively; the middle lines are the mean values of A and σ obtained by numerical averaging over each period, $2\pi n \le \omega t \le 2\pi(n+1)$; ω is the angular frequency and n is an integer. (b) Plot of the surface dilatational storage and loss moduli, E' and E'', vs. the surface pressure, π_s; E' and E'' are calculated by using sliding Fourier analysis, whereas π_s refers to the middle line of σ.

Note that the experimental oscillatory period of 5 s (Fig. 11) is small compared to the relaxation times upon expansion and compression, t_r and t_d; see Section 4. For oscillatory periods that are comparable with t_r and t_d, the relaxation processes are expected to suppress the elastic response of the surface layer. To check that, we carried out experiments at period 20 s; the obtained values of E' and E'' were about tree times smaller than those at period 5 s.

7. Conclusions

In the context of colloid and interface science, the unique properties of hydrophobins are that (i) they form adsorption layers of considerably higher surface dilatational and shear surface elasticities than the other proteins, see Fig. 10b and Ref. [4]; (ii) their

adsorption layers solidify (acquire surface shear elasticity) much faster than for the other proteins [5,7] and (iii) the hydrophobin molecules, aggregates and monolayers interact with each other with a strong hydrophobic attraction [12]. In the present study we demonstrate that these special properties essentially affect the dynamic surface tension, the rheological response to an interfacial expansion and compression, as well as the related kinetic regimes and characteristic relaxation times. Thus, the kinetics of HFBII adsorption is accelerated at higher degrees of surface coverage in contrast with the intuitive expectations that the steric hindrance of already adsorbed molecules should decelerate the adsorption. The observed effect is explained with the circumstance that the adsorbed hydrophobin molecules attract the newcomer molecules by means of the hydrophobic force (Section 4.4).

The experiments with buoyant bubbles covered with HFBII adsorption layer in pure water (Section 4.1) show that the adsorption of this protein at the air/water interface is irreversible, and that the relaxation of surface tension after an initial interfacial expansion occurs under diffusion control. Likewise, HFBII layers spread on the surface of pure water in a Langmuir trough exhibit a *diffusion* controlled relaxation after an initial expansion or compression (Section 4.2). In these cases, the surface-tension kinetics can be explained with attachment/detachment of protein molecules to/from surface aggregates limited by the surface diffusion. In view of the irreversibility of the HFBII adsorption, similar is the interpretation of the diffusion relaxation of the surface tension of HFBII solutions after *compression* (Fig. 8a). In contrast, the kinetics of relaxation of the surface tension of HFBII solutions after *expansion* occurs under *barrier* control (Fig. 7a), which is explained with the barrier to detachment (release) of protein molecules from HFBII aggregates that are present in the aqueous phase.

A sufficiently large compression leads to surface solidification, and then the surface tension remains constant after the compression (no relaxation). The deviation in the profiles of pendant drops from the Laplace shape, indicated by the computed error of the Laplace fits, unequivocally implies that the surface phase transition in the π_s-vs.-A isotherms at $\pi_s \approx 22$ mN/m is due to solidification of the HFBII adsorption layer, rather than to a buckling transition, which is observed at higher surface pressures ($\pi_s \approx 50$–60 mN/m) [46]. The solidification of the hydrophobin adsorption layer, which is composed of smaller and larger 2D aggregates, corresponds to a percolation threshold. Because at $\pi_s > 22$ mN/m the determination of surface tension by Laplace fit of the pendant drop profile is not reliable, the DSA measurements in the present article are focused on non-solidified protein adsorption layers, for which $\pi_s < 22$ mN/m.

For $\pi_s < 22$ mN/m, two different regimes of behavior of the surface dilatational elasticity, E, are observed. At the lower surface pressures, $0 < \pi_s < 11$ mN/m, predominant is the effect of increasing density of the adsorbed HFBII molecules and kinetically independent surface aggregates, so that E increases with the rise of surface pressure. In contrast, at higher surface pressures, $11 < \pi_s < 22$ mN/m, predominant is the effect of condensation of adsorbed HFBII molecules on the surface aggregates (and the merging of aggregates), so that E decreases with the rise of surface pressure.

The results can be important for the understanding and control of dynamic processes in foams [14,15] and emulsions [13,16] stabilized by hydrophobins, as well as for the modification of solid surfaces by adsorbed hydrophobin molecules [19,20,22,23].

Acknowledgments

The authors gratefully acknowledge the support from Unilever Research & Development and from the National Science Fund of Bulgaria, Grant No. DCVP 02/2-2009, UNION.

References

[1] M.B. Linder, G.R. Szilvay, T. Nakari-Setälä, M. Penttila, FEMS Microbiol. Rev. 29 (2005) 877.
[2] M. Sunde, A.H.Y. Kwan, M.D. Templeton, R.E. Beever, J.P. Mackay, Micron 39 (2008) 773.
[3] M.B. Linder, Curr. Opin. Colloid Interface Sci. 14 (2009) 356.
[4] T.B.J. Blijdenstein, P.W.N. de Groot, S.D. Stoyanov, Soft Matter 6 (2010) 1799.
[5] E.S. Basheva, P.A. Kralchevsky, N.C. Christov, K.D. Danov, S.D. Stoyanov, T.B.J. Blijdenstein, H.-J. Kim, E.G. Pelan, A. Lips, Langmuir 27 (2011) 2382.
[6] R. Borbas, B.S. Murray, E. Kiss, Colloids Surf., A 213 (2003) 93.
[7] G.M. Radulova, K. Golemanov, K.D. Danov, P.A. Kralchevsky, S.D. Stoyanov, L.N. Arnaudov, T.B.J. Blijdenstein, E.G. Pelan, A. Lips, Langmuir 28 (2012) 4168.
[8] M. Torkkeli, R. Serimaa, O. Ikkala, M. Linder, Biophys. J. 83 (2002) 2240.
[9] G.R. Szilvay, T. Nakari-Setälä, M.B. Linder, Biochemistry 45 (2006) 8590.
[10] K. Kisko, G.R. Szilvay, U. Vainio, M.B. Linder, Biophys. J. 94 (2008) 198.
[11] K. Kisko, G.R. Szilvay, E. Vuorimaa, H. Lemmetyinen, M.B. Linder, M. Torkkeli, R. Serimaa, Langmuir 25 (2009) 1612.
[12] E.S. Basheva, P.A. Kralchevsky, K.D. Danov, S.D. Stoyanov, T.B.J. Blijdenstein, E.G. Pelan, A. Lips, Langmuir 27 (2011) 4481.
[13] M. Reger, T. Sekine, T. Okamoto, H. Hoffmann, Soft Matter 7 (2011) 8248.
[14] A.R. Cox, F. Cagnol, A.B. Russell, M.J. Izzard, Langmuir 23 (2007) 7995.
[15] A.R. Cox, D.L. Aldred, A.B. Russell, Food Hydrocolloids 23 (2009) 366.
[16] F.L. Tchuenbou-Magaia, I.T. Norton, P.W. Cox, Food Hydrocolloids 23 (2009) 1877.
[17] M.B. Linder, M. Qiao, F. Laumen, K. Selber, T. Hyytiä, T. Nakari-Setälä, M.E. Penttilä, Biochemistry 43 (2004) 11873.
[18] Z.-X. Zhao, M.-Q. Qiao, F. Yin, B. Shao, B.-Y. Wu, Y.-Y. Wang, X.-S. Wang, X. Qin, S. Li, L. Yu, Q. Chen, Biosens. Bioelectron. 22 (2007) 3021.
[19] M. Qin, L.-K. Wang, X.-Z. Feng, Y.-L. Yang, R. Wang, C. Wang, L. Yu, B. Shao, M.-Q. Qiao, Langmuir 23 (2007) 4465.
[20] H. Asakawa, S. Tahara, M. Nakamichi, K. Takehara, S. Ikeno, M.B. Linder, T. Haruyama, Langmuir 25 (2009) 8841.
[21] M. Linder, G.R. Szilvay, T. Nakari-Setälä, H. Söderlund, M.E. Penttilä, Protein Sci. 11 (2002) 2257.
[22] S.O. Lumsdon, J. Green, N. Stieglitz, Colloids Surf., B 44 (2005) 172.
[23] X. Li, S. Hou, X. Feng, Y. Yu, J. Ma, L. Li, Colloids Surf., B 74 (2009) 370.
[24] J. Hakanpää, A. Paananen, S. Askolin, T. Nakari-Setälä, T. Parkkinen, M. Penttilä, M.B. Linder, J. Rouvinen, J. Biol. Chem. 279 (2004) 534.
[25] R. Miller, V.B. Fainerman, R. Wüstneck, J. Krägel, D.V. Trukhin, Colloids Surf., A 131 (1998) 225.
[26] J. Benjamins, E.H. Lucassen-Reynders, in: D. Möbius, R. Miller (Eds.), Proteins at Interfaces, Elsevier, Amsterdam, 1998 (Chapter 9).
[27] M.A. Bos, T. van Vliet, Adv. Colloid Interface Sci. 91 (2001) 437.
[28] J. Krägel, M. O'Neill, A.V. Makievski, M. Michel, M.E. Leser, R. Miller, Colloids Surf., B 31 (2003) 107.
[29] E.M. Freer, K.S. Yim, G.G. Fuller, C.J. Radke, Langmuir 20 (2004) 10159.
[30] R. Miller, V.B. Fainerman, E.V. Aksenenko, M.E. Leser, M. Michel, Langmuir 20 (2004) 771.
[31] J. Benjamins, J. Lyklema, E.H. Lucassen-Reynders, Langmuir 22 (2006) 6181.
[32] V.S. Alahverdjieva, D.O. Grigoriev, V.B. Fainerman, E.V. Aksenenko, R. Miller, H. Möhwald, J. Phys. Chem. B 112 (2008) 2136.
[33] R. Miller, J.K. Ferri, A. Javadi, J. Krägel, N. Mucic, R. Wüstneck, Colloid Polym. Sci. 288 (2010) 937.
[34] E.H. Lucassen-Reynders, J. Benjamins, V.B. Fainerman, Curr. Opin. Colloid Interface Sci. 15 (2010) 264.
[35] P.A. Wierenga, H. Gruppen, Curr. Opin. Colloid Interface Sci. 15 (2010) 365.
[36] S.C. Russev, N. Alexandrov, K.G. Marinova, K.D. Danov, N.D. Denkov, L. Lyutov, V. Vulchev, C. Bilke-Krause, Rev. Sci. Instrum. 79 (2008) 104102.
[37] N. Alexandrov, K.G. Marinova, K.D. Danov, I.B. Ivanov, J. Colloid Interface Sci. 339 (2009) 545.
[38] T.D. Gurkov, P.A. Kralchevsky, Colloids Surf. 47 (1990) 45.
[39] P.A. Kralchevsky, J.C. Eriksson, S. Ljunggren, Adv. Colloid Interface Sci. 48 (1994) 19.
[40] K.D. Danov, P.K. Kralchevsky, S.D. Stoyanov, Langmuir 26 (2010) 143.
[41] S. Usui, H. Sasaki, H. Matsukawa, J. Colloid Interface Sci. 81 (1981) 80.
[42] R.-H. Yoon, J.L. Yordan, J. Colloid Interface Sci. 113 (1986) 430.
[43] A. Graciaa, G. Morel, P. Saulnier, J. Lachaise, R.S. Schechter, J. Colloid Interface Sci. 172 (1995) 131.
[44] K.G. Marinova, R.G. Alargova, N.D. Denkov, O.D. Velev, D.N. Petsev, I.B. Ivanov, R.P. Borwankar, Langmuir 12 (1996) 2045.
[45] E. Gasteiger, C. Hoogland, A. Gattiger, S. Duvaud, M.R. Wilkins, R.D. Appel, A. Bairoch, in: J.M. Walker (Ed.), The Proteomics Protocols Handbook, Humana Press, Totowa, NJ, 2005, p. 571.
[46] E. Aumaitre, D. Vella, P. Cicuta, Soft Matter 7 (2011) 2530.
[47] G.R. Szilvay, A. Paananen, K. Laurikainen, E. Vuorimaa, H. Lemmetyinen, J. Peltonen, M.B. Linder, Biochemistry 46 (2007) 2345.
[48] A. Paananen, E. Vuorimaa, M. Torkkeli, M. Penttilä, M. Kauranen, O. Ikkala, H. Lemmetyinen, R. Serimaa, M.B. Linder, Biochemistry 42 (2003) 5253.
[49] K.L. Sutherland, Aust. J. Sci. Res. 5 (1952) 683. http://dx.doi.org/10.1071/CH9520683.
[50] P. Joos, Dynamic Surface Phenomena, V.S.P. Intl. Science, Leiden, 1999.
[51] P.A. Kralchevsky, K.D. Danov, N.D. Denkov, in: K.S. Birdi (Ed.), Handbook of Surface and Colloid Chemistry, CRC Press, Boca Raton, 2009, p. 197 (Chapter 7).
[52] T.D. Gurkov, K.G. Marinova, A. Zdravkov, C. Oleksiak, B. Campbell, Prog. Colloid Polym. Sci. 110 (1998) 263, http://dx.doi.org/10.1007/BFb0118089.

[53] J.B. Li, G. Kretzschmar, R. Miller, H. Möhwald, Colloids Surf., A 149 (1999) 491.
[54] K.D. Danov, D.S. Valkovska, P.A. Kralchevsky, J. Colloid Interface Sci. 251 (2002) 18.
[55] J. Hakanpää, G.R. Szilvay, H. Kaljunen, M. Maksimainen, M. Linder, J. Rouvinen, Protein Sci. 15 (2006) 2129.
[56] J.M. Kallio, M.B. Linder, J. Rouvinen, J. Biol. Chem. 282 (2007) 28733.
[57] P.A. Wierenga, M.B.J. Meinders, M.R. Egmond, A.G.J. Voragen, H.H.J. de Jongh, J. Phys. Chem. B 109 (2005) 16946.
[58] S. Damodaran, K.B. Song, ACS Symp. Ser. 454 (1991) 104.
[59] N.C. Christov, D.N. Ganchev, N.D. Vassileva, N.D. Denkov, K.D. Danov, P.A. Kralchevsky, Colloids Surf., A 209 (2002) 83.
[60] K. Koczo, A.D. Nikolov, D.T. Wasan, R.P. Borwankar, A. Gonsalves, J. Colloid Interface Sci. 178 (1996) 694.
[61] J.W. Gibbs, The Scientific Papers of J.W. Gibbs, vol. 1, Dover, New York, 1961.
[62] R. Aveyard, J.H. Clint, D. Nees, V.N. Paunov, Langmuir 16 (2000) 1969.
[63] S. Reynaert, P. Moldenaers, J. Vermant, Langmuir 22 (2006) 4936.
[64] J. Lucassen, M. van den Tempel, Chem. Eng. Sci. 27 (1972) 1283.
[65] F. Ravera, G. Loglio, P. Pandolfini, E. Santini, L. Liggieri, Colloids Surf., A 365 (2010) 2.
[66] F. Ravera, G. Loglio, V.I. Kovalchuk, Curr. Opin. Colloid Interface Sci. 15 (2010) 217.
[67] I.B. Ivanov, K.D. Danov, K.P. Ananthapadmanabhan, A. Lips, Adv. Colloid Interface Sci. 114 (2005) 61.